Nanocomposite dispersion in melt mixers

Danielle Veigel[1,2], Kabir Rishi[3], Ugochukwu Okoli[1], Gregory Beaucage[1*], Jeffery A. Galloway[2], Hannah Campanelli[1,2], Jan Ilavsky[4], Ivan Kuzmenko[4], Melodie Fickenscher[5]

[1]Chemical & Materials Engineering, University of Cincinnati, Cincinnati OH 45221, USA
[2]KraussMaffei, Florence, KY 41042, USA
[3]Centers for Disease Control and Prevention, National Institute for Occupational Safety and Health, Cincinnati, OH 45213, USA
[4]X-Ray Science Division, Advanced Photon Source, Argonne National Laboratory, Lemont IL 60439, USA
[5]Advanced Materials Characterization Center, College of Engineering & Applied Sciences, University of Cincinnati, Cincinnati OH 45221, USA

Supplementary Information

Table A1. Fit Parameters for $I_0(q)/\phi_0$ curves fit using equation 1 for carbon black/polystyrene samples processed on the twin-screw extruder (GM-300, GM-400, KB-300, KB-400), single-screw extruder (SSE) and Brabender Mixer.

	Level 1 (Primary Particle)				Level 2 (Aggregates)			
Sample ID	G_1/ϕ_0 (10^4 cm^{-1})	$R_{g,1}$ (Å)	B_1/ϕ_0 (10^{-4} cm^{-1}Å^{-4})	P_1	G_2/ϕ_0 (10^6 cm^{-1})	$R_{g,2}$ (Å)	B_2/ϕ_0 (cm^{-1}Å^{-P2})	P_2
GM-300	4 (±2)	190 (±20)	3.2 (±0.2)	4	2.6 (±0.08)	1100 (±40)	0.7 (±0.3)	2.3 (±0.1)
GM-400	4 (±2)	200 (±30)	2.9 (±0.3)	4	4.0 (±0.3)	1600 (±140)	1.0 (±0.7)	2.2 (±0.1)
KB-300	3 (±1)	180 (±20)	3.5 (±0.2)	4	2.6 (±0.1)	1040 (±50)	0.6 (±0.2)	2.4 (±0.1)
KB-400	3 (±1)	190 (±20)	3.0 (±0.2)	4	3.6 (±0.1)	1400 (±50)	0.5 (±0.2)	2.3 (±0.1)
SSE	5 (±1)	270 (±10)	1.2 (±0.03)	4	3.1 (±1)	2400 (±800)	0.6 (±0.4)	2.1 (±0.1)
Mixer	11 (±4)	280 (±30)	2.3 (±0.1)	4	5.4 (±1)	2000 (±600)	1.0 (±1.0)	2.2 (±0.2)

Table A2. Primary particle size (d_{p}) and the associated polydispersity (PDI), the aggregate size (R_{eted}), the degree of aggregation (z), the number of primary particles along the short circuit path (p), aggregate topological parameters ($d_{\mathrm{f}}, d_{\mathrm{min}}$, and c), and the branch fraction (ϕ_{br}) from the fit parameters in Table A1 for carbon black/polystyrene samples processed on the twin-screw extruder (A-GM-300, A-GM-400, B-KB-300, B-KB-400), single-screw extruder (SSE) and Brabender Mixer. R is defined as a dimensionless parameter expressed as the ratio of R_{eted} and d_{p}.

Sample ID	d_{p} (nm)	PDI	R_{eted} (nm)	$R = \frac{R_{\mathrm{eted}}}{d_{\mathrm{p}}}$	z	p	d_{f}	d_{min}	c	ϕ_{br}
GM-300	19 (±1)	7	120 (±15)	6 (±1)	70 (±20)	11 (±2)	2.3 (±0.1)	1.3 (±0.3)	1.8 (±0.5)	0.85 (±0.4)
	Simulation result (P=0.81[a])			8.9[b]	69[a]	13[b]	1.94[b]	1.19[b]	1.63[b]	0.81[b]
GM-400	20 (±2)	8	150 (±30)	8 (±2)	100 (±40)	17 (±4)	2.2 (±0.1)	1.4 (±0.5)	1.6 (±0.6)	0.83 (±0.5)
	Simulation result (P=0.74[a])			10.2[b]	100[a]	21[b]	1.99[b]	1.31[b]	1.52[b]	0.79[b]
KB-300	17 (±1)	7	110 (±10)	7 (±1)	90 (±20)	11 (±1)	2.4 (±0.1)	1.2 (±0.2)	1.9 (±0.3)	0.88 (±0.3)
	Simulation result (P=0.89[a])			10.7[b]	91[a]	16[b]	1.90[b]	1.18[b]	1.61[b]	0.82[b]
KB-400	18 (±1)	8	140 (±15)	8 (±1)	120 (±20)	16 (±2)	2.3 (±0.1)	1.4 (±0.5)	1.7 (±0.6)	0.86 (±0.2)
	Simulation result (P=0.57[a])			10.9[b]	116[a]	23[b]	1.99[b]	1.31[b]	1.52[b]	0.80[b]
SSE	25 (±1)	8	190 (±20)	8 (±1)	70 (±12)	26 (±4)	2.1 (±0.1)	1.6 (±0.8)	1.3 (±0.6)	0.62 (±0.2)
	Simulation result (P=0.47[a])			8.6[b]	68[a]	20[b]	1.96[b]	1.40[b]	1.40[b]	0.70[b]
Mixer	26 (±1)	8	160 (±15)	6 (±1)	48 (±7)	24 (±3)	2.2 (±0.2)	1.8 (±1)	1.2 (±0.8)	0.50 (±0.2)
	Simulation result (P=0.10[a])			6.7[b]	48[a]	26[b]	2.0[b]	1.71[b]	1.19[b]	0.46[b]

[a] input values for simulation; P indicates sticking probability of the spherical primary particles while z indicates the number of primary particles in an aggregate on average.

[b] output values for the simulated aggregates

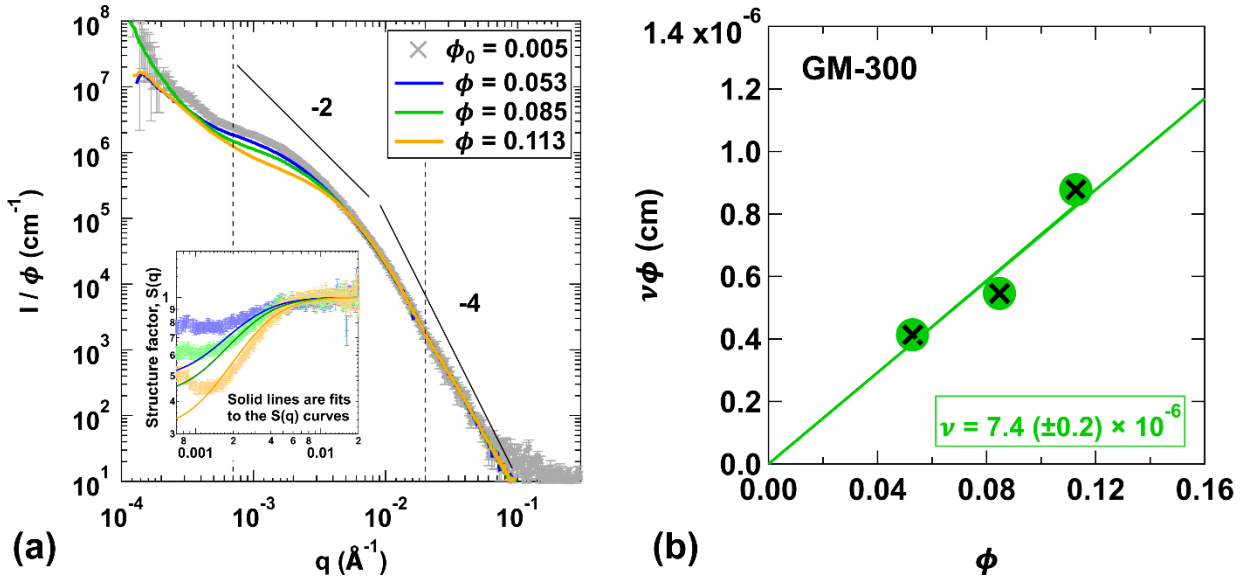

Figure S1. USAXS curves for carbon black/polystyrene nanocomposite processed in the twin-screw extruder operated at 300 rpm with screw design utilizing GM. The dilute scattering curve, $I_0(q)/\phi_0$, was fit using equation 1 for $0.0007\text{Å}^{-1} < q < 0.02\text{Å}^{-1}$, i.e., the region within the dashed lines. Increasing filler concentration results in a reduction in the $I(q)/\phi$ curves in the region associated with the aggregate structural level between the dashed lines indicating aggregate overlap. The corresponding structure factor, $S(q)$, obtained by normalizing $I(q)/\phi$ by $I_0(q)/\phi_0$ within this region is shown in the inset figure. These $S(q)$ curves were fit using equation 3 to quantify the extent of screening/overlap, $\phi\nu$. (b) A plot of $\phi\nu$ as a function of the filler concentration ϕ to determine the effective interaction parameter, ν.

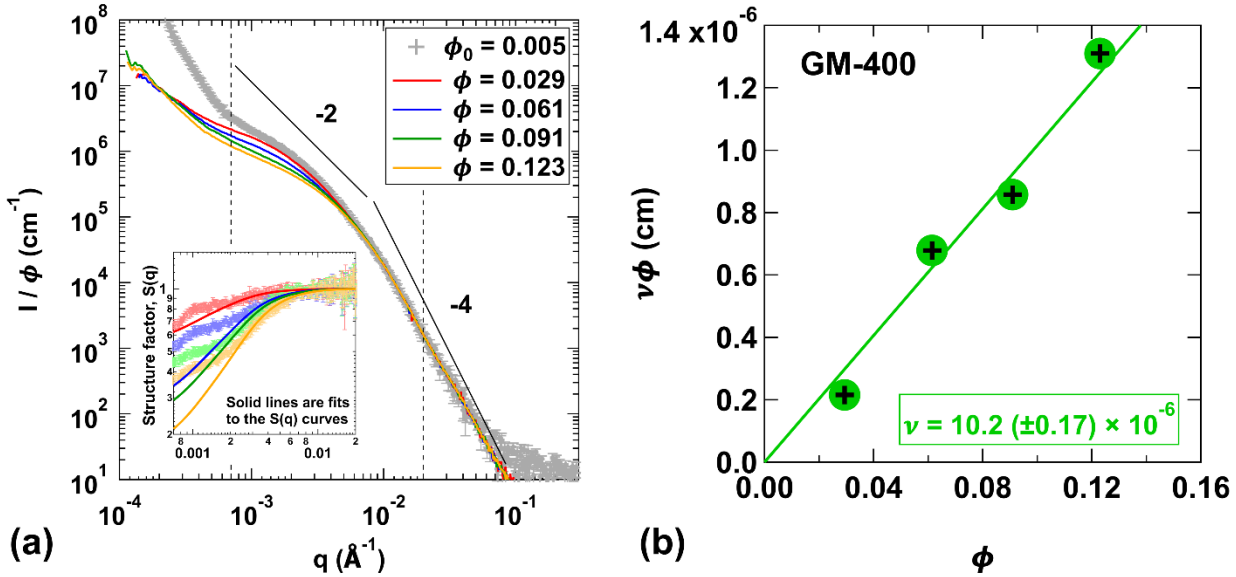

Figure S2. USAXS curves for carbon black/polystyrene nanocomposite processed in the twin-screw extruder operated at 400 rpm with screw design utilizing GM. The dilute scattering curve, $I_0(q)/\phi_0$, was fit using equation 1 for $0.0007\text{Å}^{-1} < q < 0.02\text{Å}^{-1}$, i.e., the region within the dashed lines. Increasing filler concentration results in a reduction in the $I(q)/\phi$ curves in the region associated with the aggregate structural level between the dashed lines indicating aggregate overlap. The corresponding structure factor, $S(q)$, obtained by normalizing $I(q)/\phi$ by $I_0(q)/\phi_0$ within this region is shown in the inset figure. These $S(q)$ curves were fit using equation 3 to quantify the extent of screening/overlap, $\phi\nu$. (b) A plot of $\phi\nu$ as a function of the filler concentration ϕ to determine the effective interaction parameter, ν.

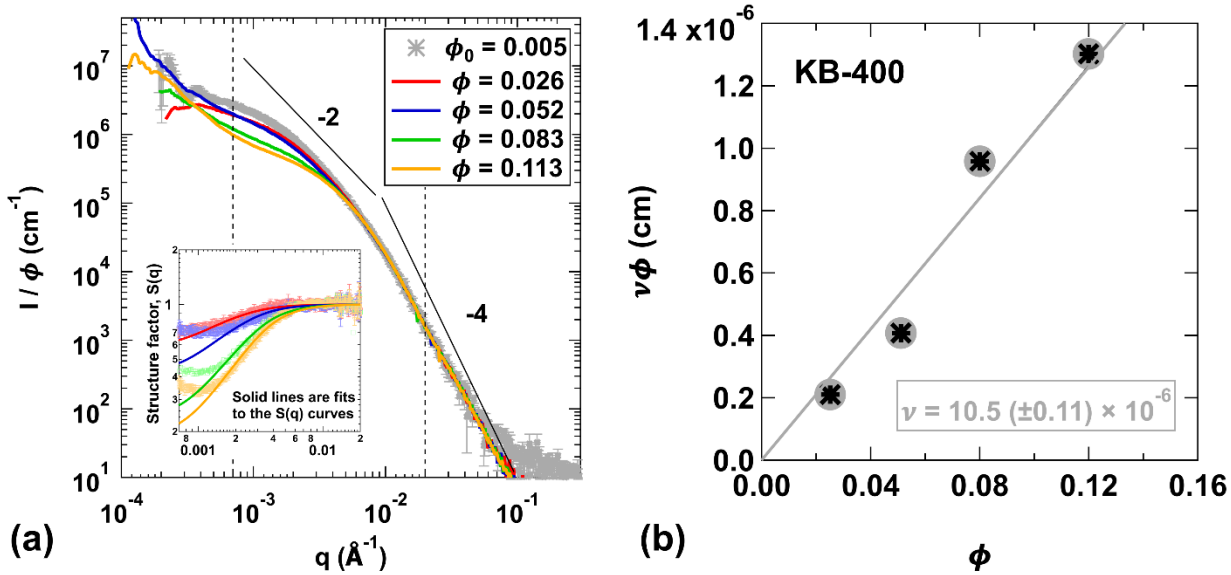

Figure S3. USAXS curves for carbon black/polystyrene nanocomposite processed in the twin-screw extruder operated at 400 rpm with screw design utilizing KB. The dilute scattering curve, $I_0(q)/\phi_0$, was fit using equation 1 for $0.0007\text{Å}^{-1} < q < 0.02\text{Å}^{-1}$, i.e., the region within the dashed lines. Increasing filler concentration results in a reduction in the $I(q)/\phi$ curves in the region associated with the aggregate structural level between the dashed lines indicating aggregate overlap. The corresponding structure factor, $S(q)$, obtained by normalizing $I(q)/\phi$ by $I_0(q)/\phi_0$ within this region is shown in the inset figure. These $S(q)$ curves were fit using equation 3 to quantify the extent of screening/overlap, $\phi\nu$. (b) A plot of $\phi\nu$ as a function of the filler concentration ϕ to determine the effective interaction parameter, ν.

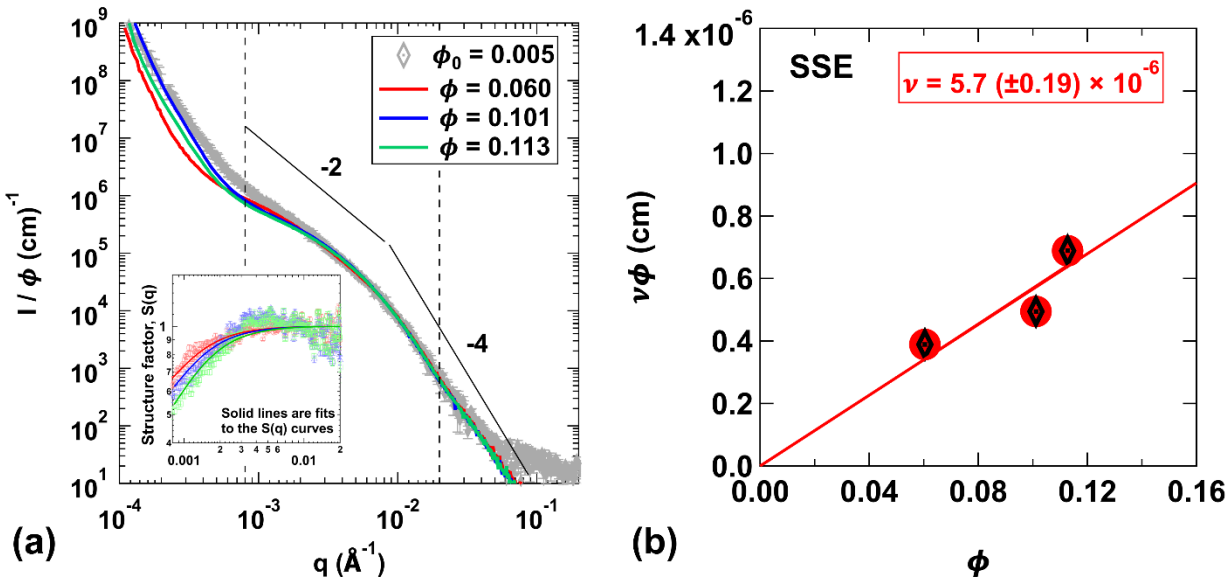

Figure S4. USAXS curves for carbon black/polystyrene nanocomposite processed in the single screw extruder (SSE) operated at 30 rpm. The dilute scattering curve, $I_0(q)/\phi_0$, was fit using equation 1 for $0.0008\text{Å}^{-1} < q < 0.02\text{Å}^{-1}$, i.e., the region within the dashed lines. Increasing filler concentration results in a reduction in the $I(q)/\phi$ curves in the region associated with the aggregate structural level between the dashed lines indicating aggregate overlap. The corresponding structure factor, $S(q)$, obtained by normalizing $I(q)/\phi$ by $I_0(q)/\phi_0$ within this region is shown in the inset figure. These $S(q)$ curves were fit using equation 3 to quantify the extent of screening/overlap, $\phi\nu$. (b) A plot of $\phi\nu$ as a function of the filler concentration ϕ to determine the effective interaction parameter, ν.

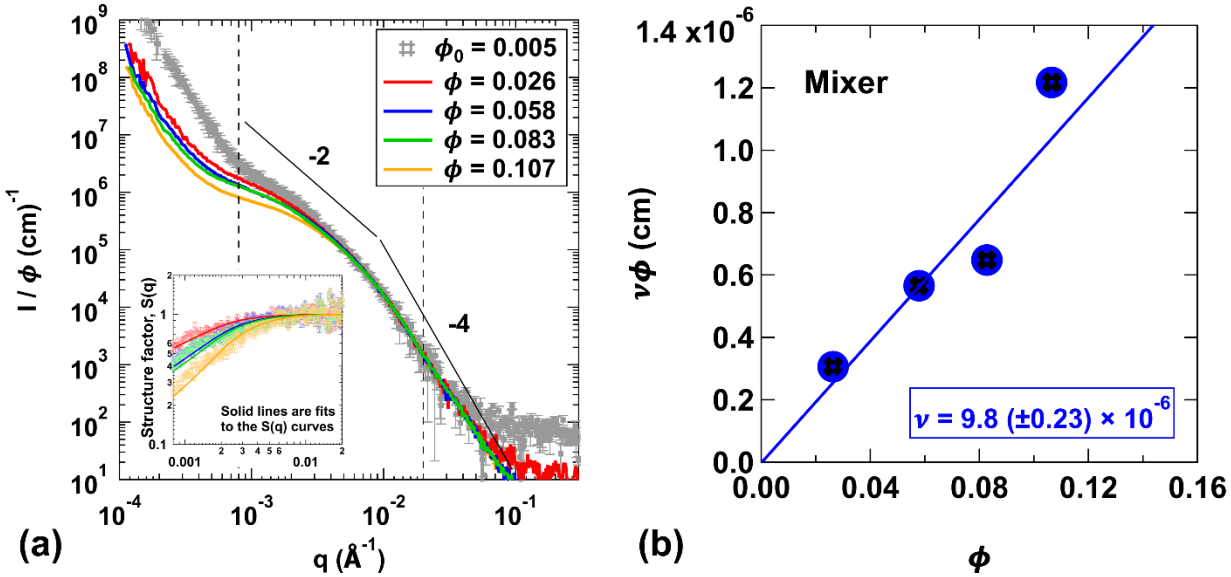

Figure S5. USAXS curves for carbon black/polystyrene nanocomposite processed in the Mixer operated at 60 rpm. The dilute scattering curve, $I_0(q)/\phi_0$, was fit using equation 1 for $0.0008\text{Å}^{-1} < q < 0.02\text{Å}^{-1}$, i.e., the region within the dashed lines. Increasing filler concentration results in a reduction in the $I(q)/\phi$ curves in the region associated with the aggregate structural level between the dashed lines indicating aggregate overlap. The corresponding structure factor, $S(q)$, obtained by normalizing $I(q)/\phi$ by $I_0(q)/\phi_0$ within this region is shown in the inset figure. These $S(q)$ curves were fit using equation 3 to quantify the extent of screening/overlap, $\phi\nu$. (b) A plot of $\phi\nu$ as a function of the filler concentration ϕ to determine the effective interaction parameter, ν.

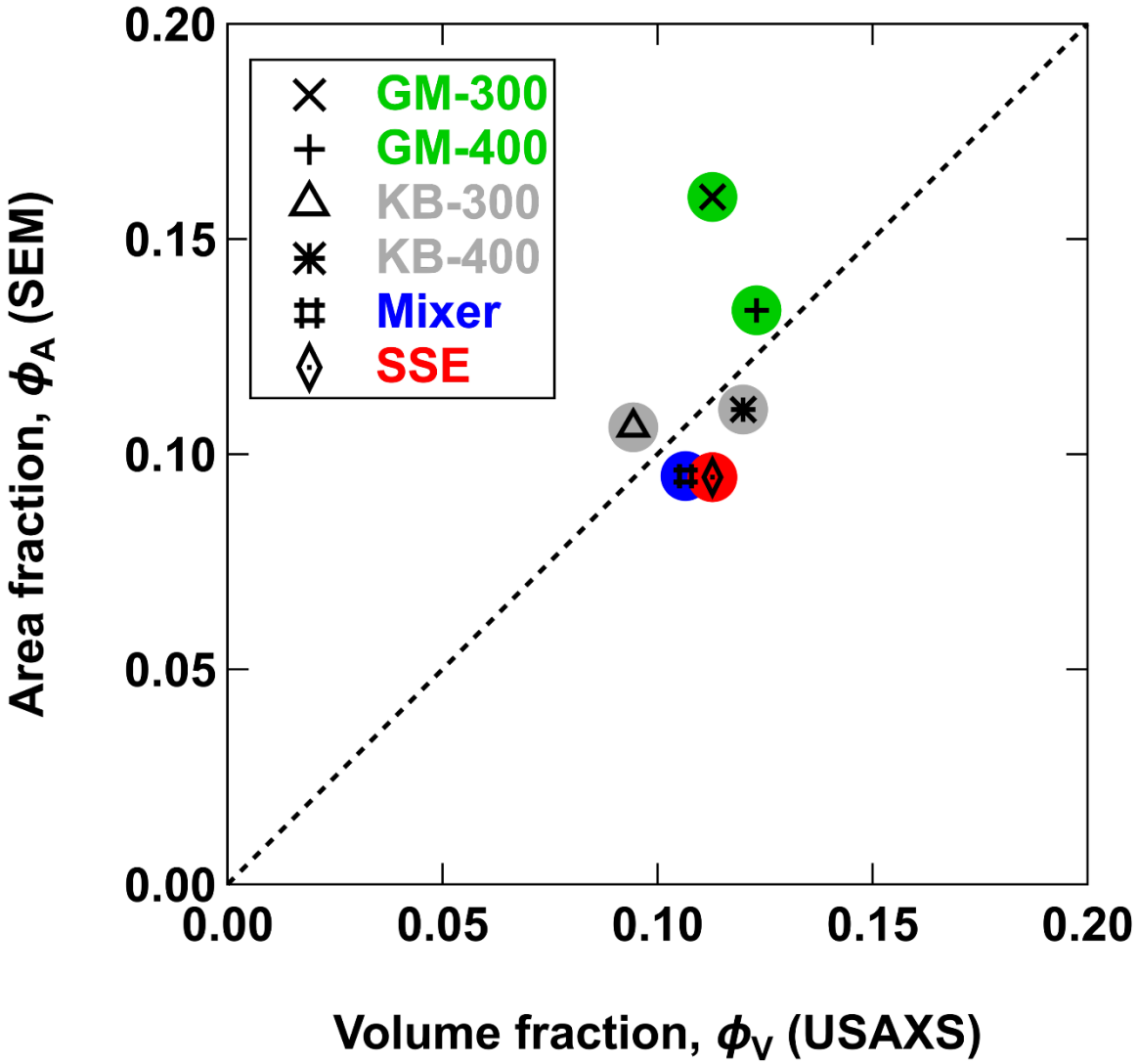

Figure S6. A comparison of the area fraction from SEM micrograph analysis in Figure 5, ϕ_A, and the volume fraction, ϕ_V, from scattering for the carbon black fillers in polystyrene. A linear relationship indicated by the dashed line indicates agreement between the two measurement methods at two length scales, macroscopic for ϕ_A and nanoscale for ϕ_V. A strong deviation for GM-300 (green "×" symbol) is attributed to the surface asperities in the SEM micrographs, which could not be completely removed during image processing in Figure 4.

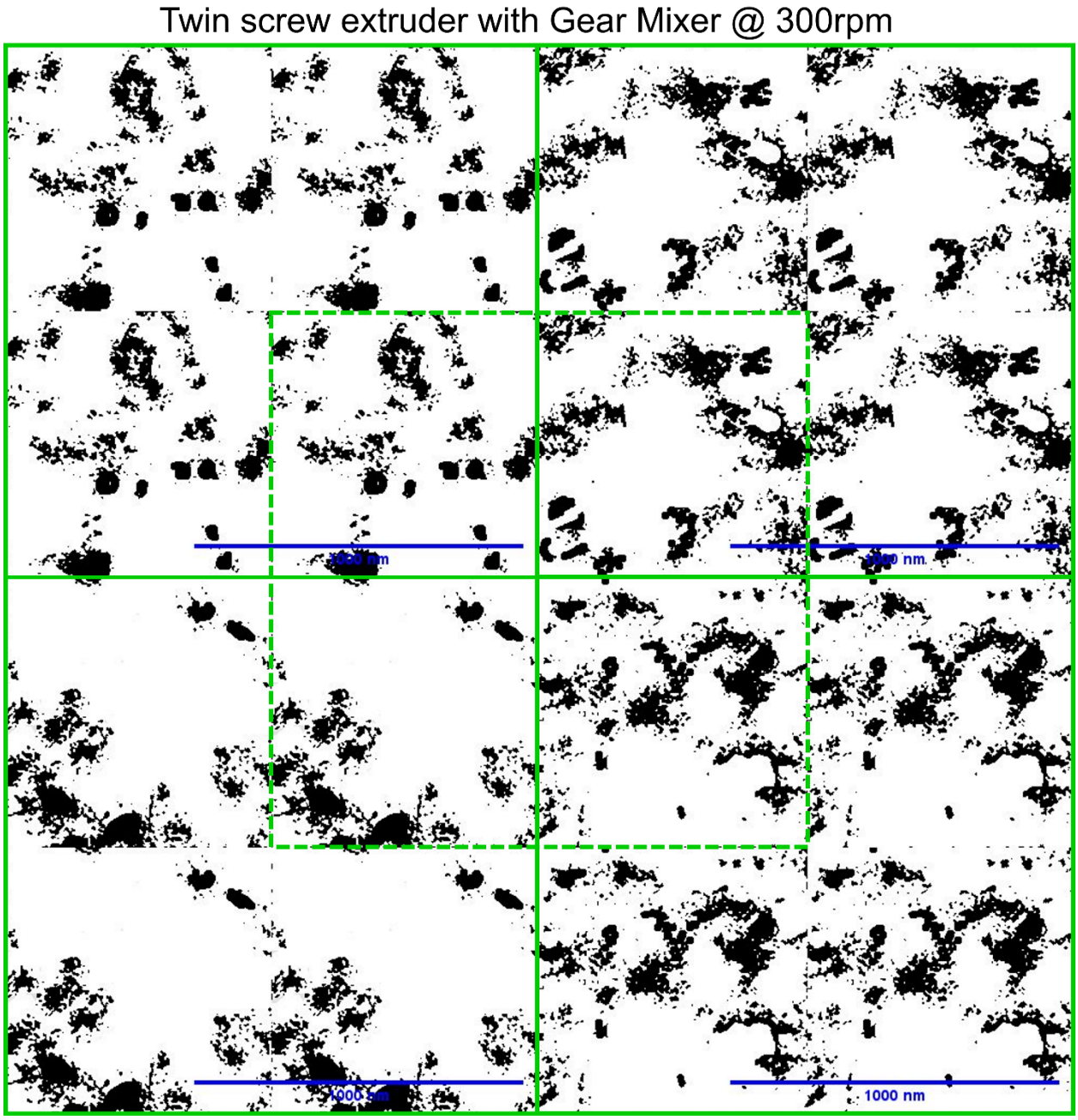

Figure S7. Four images (see corners) constructed from the corner sections of the processed binary image for GM-300 (center image, also shown in Figure 4(a) in the main text). These images were utilized to determine $L_{\mathrm{f,avg}}$ and the associated error.

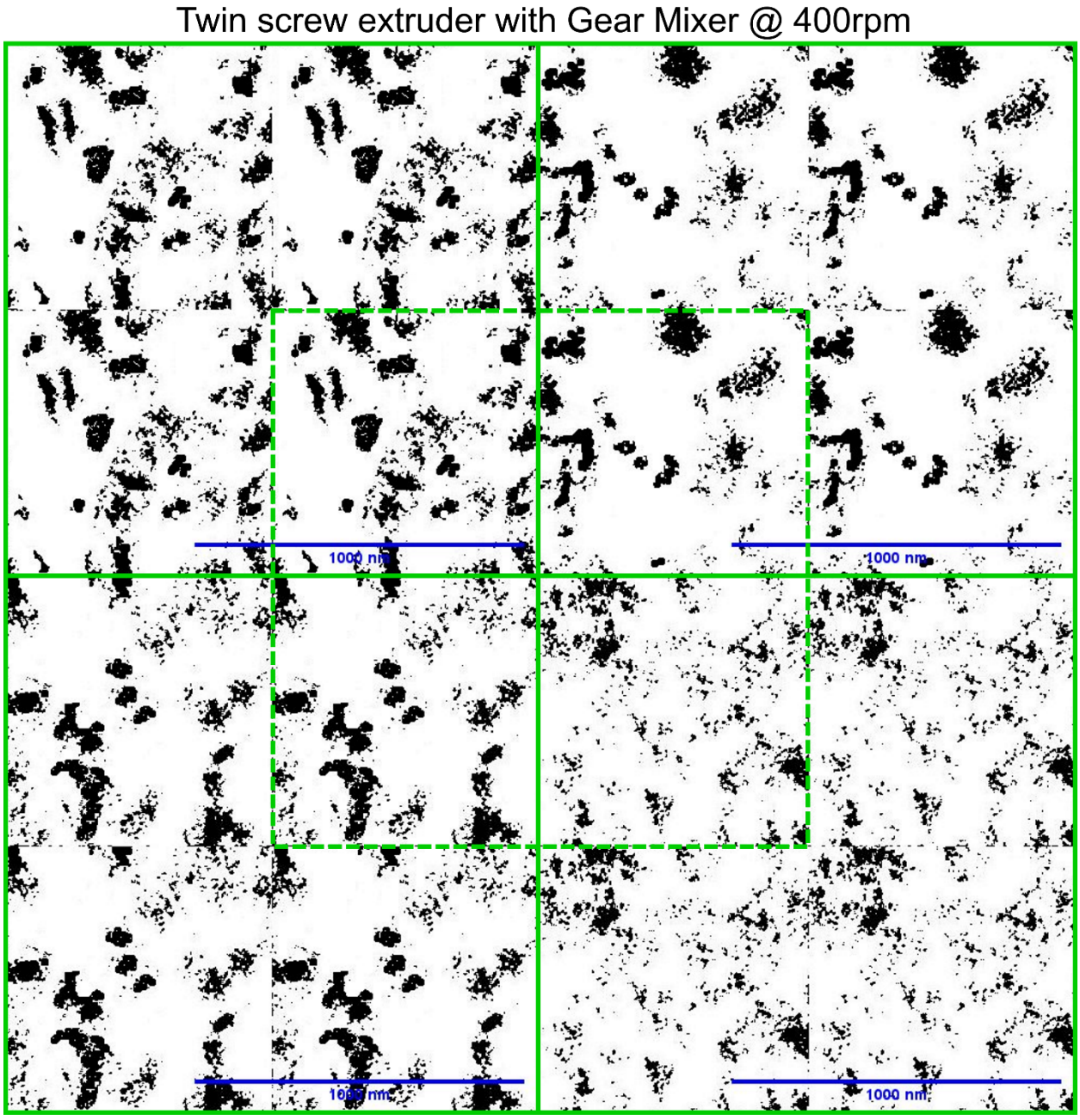

Figure S8. Four images (see corners) constructed from the corner sections of the processed binary image for GM-400 (center image, also shown in Figure 4(b) in the main text). These images were utilized to determine $L_{\mathrm{f,avg}}$ and the associated error.

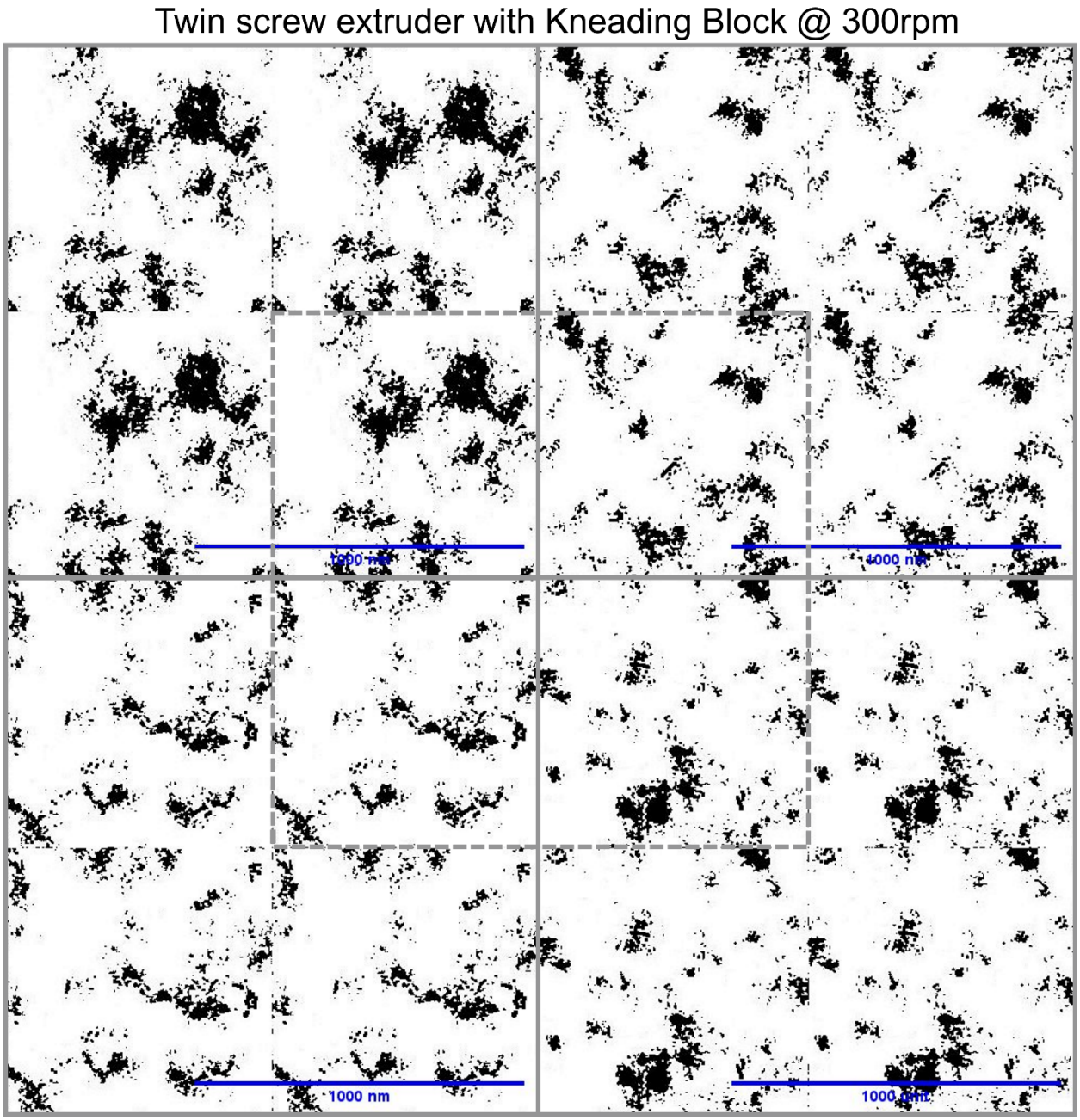

Figure S9. Four images (see corners) constructed from the corner sections of the processed binary image for KB-300 (center image, also shown in Figure 4(c) in the main text). These images were utilized to determine $L_{\mathrm{f,avg}}$ and the associated error.

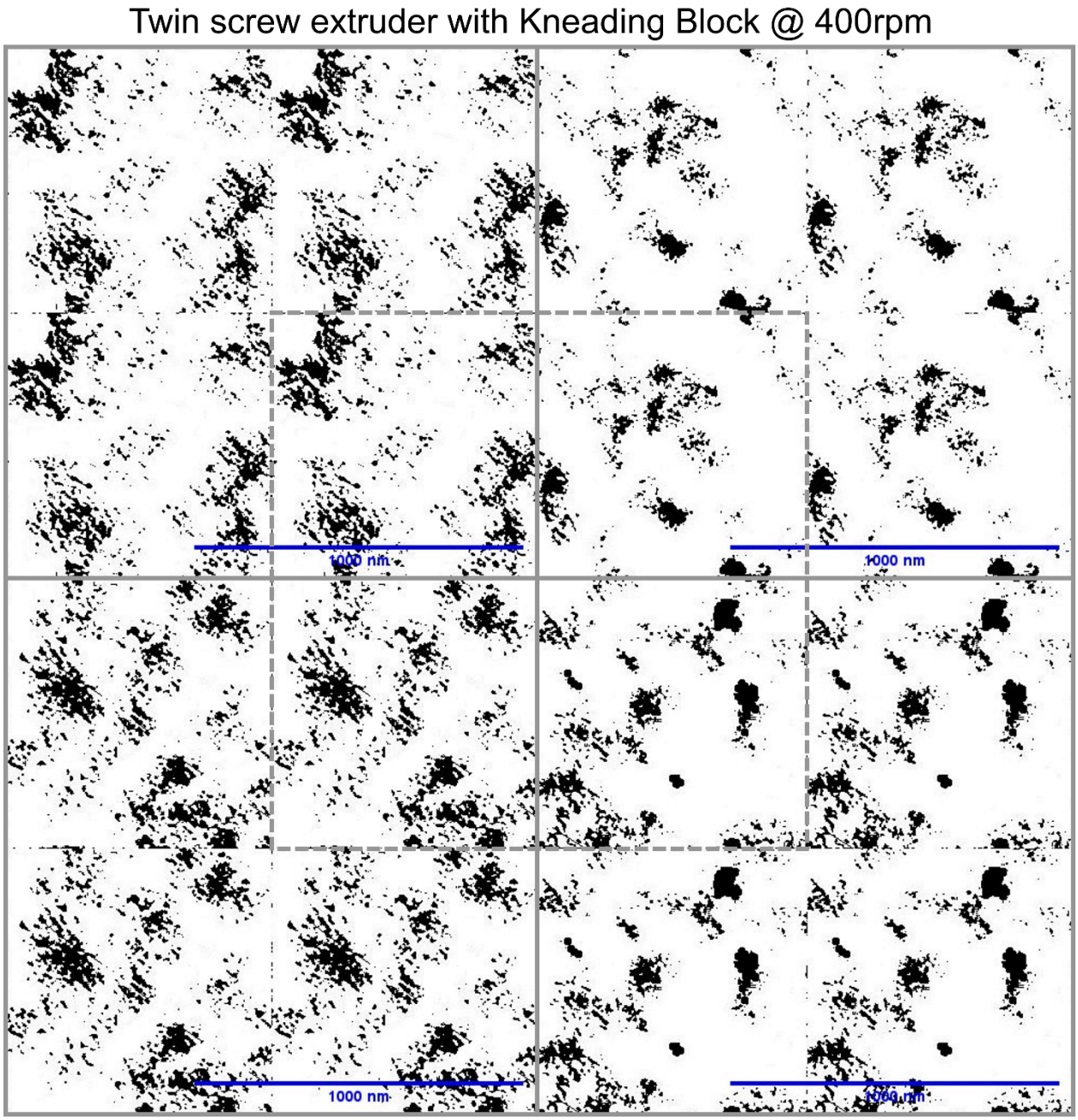

Figure S10. Four images (see corners) constructed from the corner sections of the processed binary image for KB-400 (center image, also shown in Figure 4(d) in the main text). These images were utilized to determine $L_{\mathrm{f,avg}}$ and the associated error.

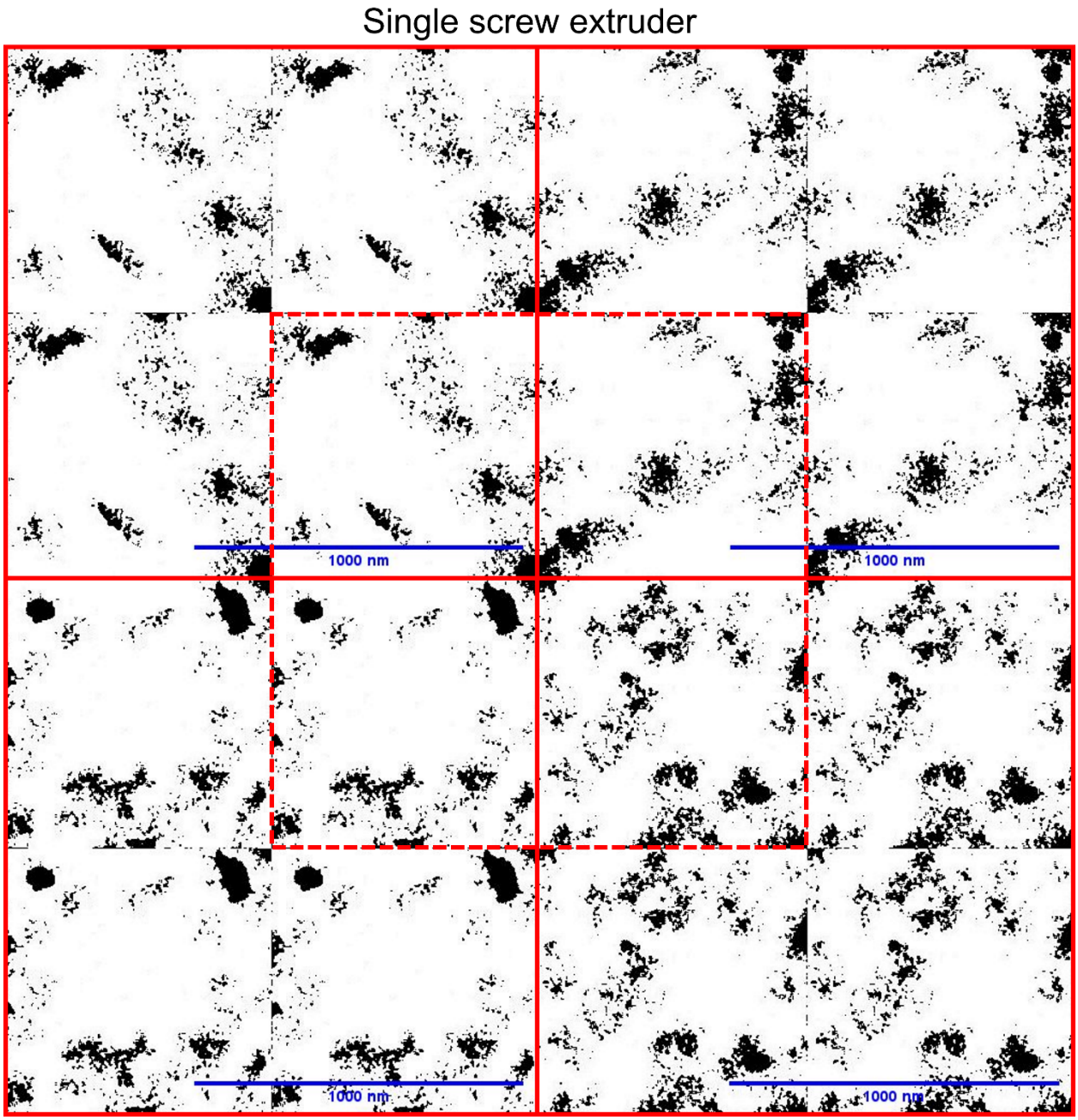

Figure S11. Four images (see corners) constructed from the corner sections of the processed binary image for SSE (center image, also shown in Figure 4(e) in the main text). These images were utilized to determine $L_{\mathrm{f,avg}}$ and the associated error.

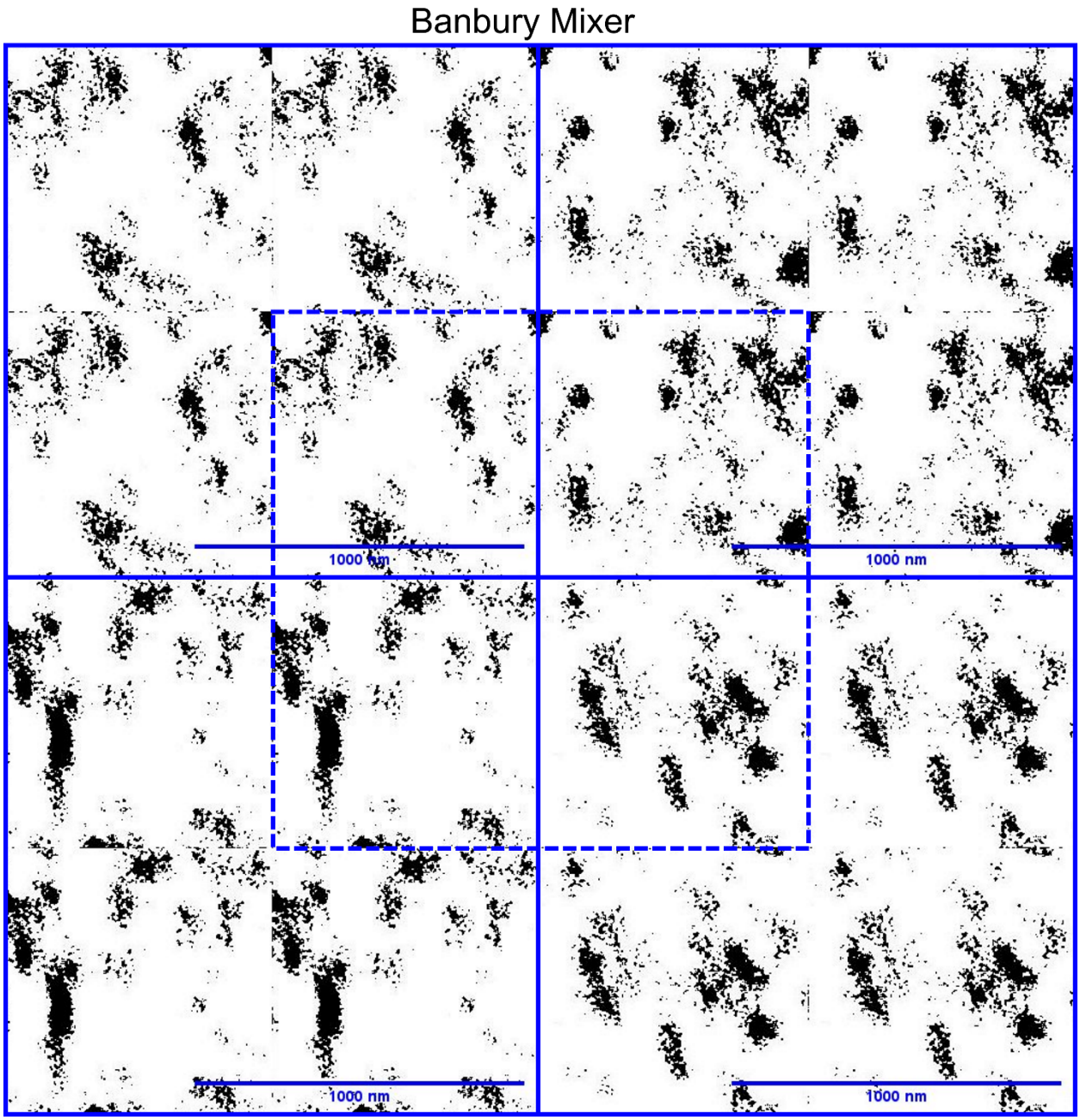

Figure S12. Four images (see corners) constructed from the corner sections of the processed binary image for Mixer (center image, also shown in Figure 4(f) in the main text). These images were utilized to determine $L_{\mathrm{f,avg}}$ and the associated error.